

## Shape Optimal Design on Double-Chamber Mufflers Using Simulated Annealing and a Genetic Algorithm

Long-Jyi YEH, Ying-Chun CHANG , Min-Chie CHIU  
*Tatung University, Department of Mechanical Engineering,  
Taipei, Taiwan R.O.C.  
e-mail: min-chie.chiu@ctci.com.tw*

Received 22.03.2004

### Abstract

Whilst the space volume of mufflers in a noise control system is often constrained for maintenance and operation in practical engineering work, the maximization of the muffler's performance becomes essential. In this paper, both simulated annealing (SA) and a genetic algorithm (GA) are applied simultaneously. A numerical case of pure tone noise control is introduced. Before optimization, one example is tested and compared with the experimental data for the accuracy check of the mathematical model. The results reveal that the GA is more accurate than SA during the optimal process with a fixed iteration. Under space constraints, this approach provides a quick and novel scheme for the design of double-chamber mufflers.

**Key words:** Double-chamber muffler, Four-pole matrix method, Sound transmission loss, Space constraints, Simulated annealing.

### Introduction

As investigated by the Occupational Safety and Health Act (OSHA) of 1970, high noise levels can be harmful to workers and can lead not only to psychological but also to physiological ailments (Cheremisinoff, 1977). Therefore, the strategy of noise control on equipment becomes important. Mufflers are normally used in eliminating noise from venting systems (Magrab and Edward, 1975). However, the space of mufflers is often limited to operation and maintenance requirements. Even if many studies on muffler designs have been conducted, the discussion of optimal designs under space constraints is rarely emphasized. In the previous work by Yeh et al. (2002), the graphical analysis of optimal shape designs (aimed to improve the performance of sound transmission loss (STL) on a constrained single expansion muffler) was discussed. In order to enhance the STL on muffler, the shape optimization of constrained double-chamber mufflers (with extended tubes by mathematical gradient methods) was explored and discussed by Yeh et al. (2003). However, it is trou-

blesome to look for a good starting point in different gradient-based optimal processes even in the exterior penalty function method or in the interior penalty function method. Therefore, new optimizers, simulated annealing (SA) and genetic algorithm (GA), were introduced.

SA, a stochastic relaxation technique oriented by Metropolis et al. (1983) and developed by Kirkpatrick et al. (1953), imitates the physical process of annealing metal to reach the minimum energy state. The GA, a stochastic algorithm, is used as an optimizer by mimicking genetic drift and the Darwinian strife for survival.

Unlike the traditional gradient-based method, which needs the derivatives and a good starting point in the objective function, both the SA and GA optimizers have a good opportunity to locate the global optimum in a near optimal manner. In this paper, SA and a GA are coupled with the transfer matrix method (based on the plane wave theory) in order to optimize the performance of mufflers on constrained venting systems.

**Theoretical Background**

A 3-D cross-section view of the double-chamber muffler is shown in Figure 1. As depicted in Figure 2, 3 elements of straight ducts and 2 elements of ex-

pansion/contraction ducts are identified. The whole flow condition within the muffler represented by 10 chosen nodes (pt1~pt10) is shown in Figure 3. The individual transfer matrix in each element is simply expressed as

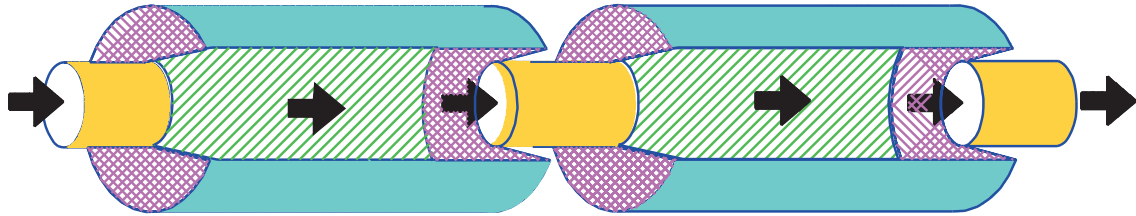


**Figure 1.** 3-D cross-section for a double-chamber muffler.

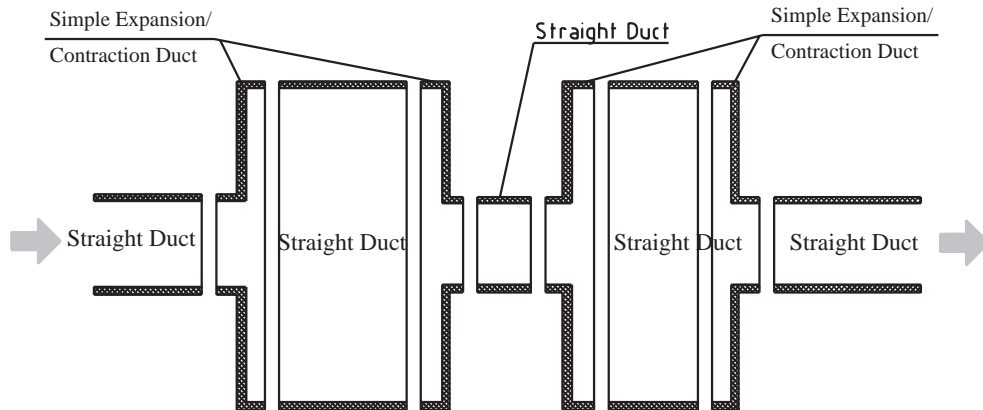


**Figure 2.** Distinguishing of muffler elements.

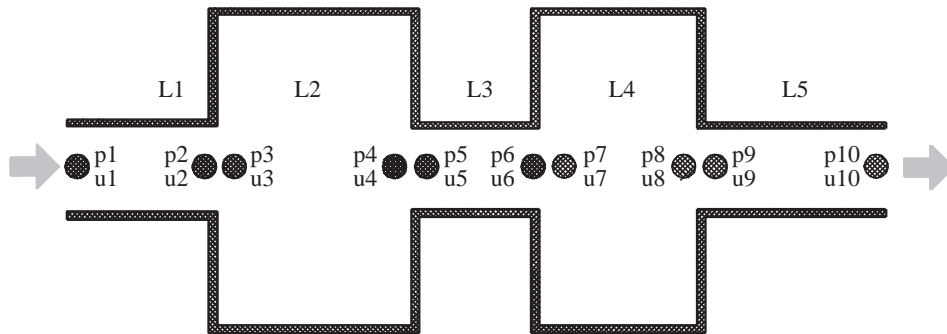


**Figure 3.** Flow condition for a double-chamber muffler.

$$\begin{pmatrix} p_1 \\ \rho_o c_o u_1 \end{pmatrix} = e^{-jM_1 k L_1 / (1 - M_1^2)} \begin{bmatrix} b_{11} & b_{12} \\ b_{21} & b_{22} \end{bmatrix} \begin{pmatrix} p_2 \\ \rho_o c_o u_2 \end{pmatrix} \quad (1)$$

$$\begin{pmatrix} p_2 \\ \rho_o c_o u_2 \end{pmatrix} = \begin{bmatrix} 1 & 0 \\ 0 & \frac{S_2}{S_1} \end{bmatrix} \begin{pmatrix} p_3 \\ \rho_o c_o u_3 \end{pmatrix} \quad (2)$$

$$\begin{pmatrix} p_3 \\ \rho_o c_o u_3 \end{pmatrix} = e^{-jM_2 k L_2 / (1-M_2^2)} \begin{bmatrix} c11 & c12 \\ c21 & c22 \end{bmatrix} \begin{pmatrix} p_4 \\ \rho_o c_o u_4 \end{pmatrix} \quad (3)$$

$$\begin{pmatrix} p_4 \\ \rho_o c_o u_4 \end{pmatrix} = \begin{bmatrix} 1 & 0 \\ 0 & \frac{S_3}{S_2} \end{bmatrix} \begin{pmatrix} p_5 \\ \rho_o c_o u_5 \end{pmatrix} \quad (4)$$

$$\begin{pmatrix} p_5 \\ \rho_o c_o u_5 \end{pmatrix} = e^{-jM_3 k L_3 / (1-M_3^2)} \begin{bmatrix} d11 & d12 \\ d21 & d22 \end{bmatrix} \begin{pmatrix} p_6 \\ \rho_o c_o u_6 \end{pmatrix} \quad (5)$$

$$\begin{pmatrix} p_6 \\ \rho_o c_o u_6 \end{pmatrix} = \begin{bmatrix} 1 & 0 \\ 0 & \frac{S_4}{S_3} \end{bmatrix} \begin{pmatrix} p_7 \\ \rho_o c_o u_7 \end{pmatrix} \quad (6)$$

$$\begin{pmatrix} p_7 \\ \rho_o c_o u_7 \end{pmatrix} = e^{-jM_4 k L_4 / (1-M_4^2)} \begin{bmatrix} e11 & e12 \\ e21 & e22 \end{bmatrix} \begin{pmatrix} p_8 \\ \rho_o c_o u_8 \end{pmatrix} \quad (7)$$

$$\begin{pmatrix} p_8 \\ \rho_o c_o u_8 \end{pmatrix} = \begin{bmatrix} 1 & 0 \\ 0 & \frac{S_5}{S_4} \end{bmatrix} \begin{pmatrix} p_9 \\ \rho_o c_o u_9 \end{pmatrix} \quad (8)$$

$$\begin{pmatrix} p_9 \\ \rho_o c_o u_9 \end{pmatrix} = e^{-jM_5 k L_5 / (1-M_5^2)} \begin{bmatrix} f11 & f12 \\ f21 & f22 \end{bmatrix} \begin{pmatrix} p_{10} \\ \rho_o c_o u_{10} \end{pmatrix} \quad (9)$$

Full descriptions of the transfer matrix in the straight duct and in the simple expansion/contraction duct are also specified in appendices A and B. Using matrix substitution on Eqs. (1)-(9), the complete system matrix is

$$\begin{aligned} \begin{pmatrix} p_1 \\ \rho_o c_o u_1 \end{pmatrix} &= e^{-jk(\frac{M_1 L_1}{1-M_1^2} + \frac{M_2 L_2}{1-M_2^2} + \frac{M_3 L_3}{1-M_3^2} + \frac{M_4 L_4}{1-M_4^2} + \frac{M_5 L_5}{1-M_5^2})} \begin{bmatrix} b11 & b12 \\ b21 & b22 \end{bmatrix} \begin{bmatrix} 1 & 0 \\ 0 & \frac{S_2}{S_1} \end{bmatrix} \begin{bmatrix} c11 & c12 \\ c21 & c22 \end{bmatrix} \\ &\begin{bmatrix} 1 & 0 \\ 0 & \frac{S_3}{S_2} \end{bmatrix} \begin{bmatrix} d11 & d12 \\ d21 & d22 \end{bmatrix} \begin{bmatrix} 1 & 0 \\ 0 & \frac{S_4}{S_3} \end{bmatrix} \begin{bmatrix} e11 & e12 \\ e21 & e22 \end{bmatrix} \begin{bmatrix} 1 & 0 \\ 0 & \frac{S_5}{S_4} \end{bmatrix} \begin{bmatrix} f11 & f12 \\ f21 & f22 \end{bmatrix} \begin{pmatrix} p_{10} \\ \rho_o c_o u_{10} \end{pmatrix} \\ &= \begin{bmatrix} T11 & T12 \\ T21 & T22 \end{bmatrix} \begin{pmatrix} p_{10} \\ \rho_o c_o u_{10} \end{pmatrix} \end{aligned} \quad (10)$$

Consequently, the STL of a muffler (Munjaj, 1987) is

$$\begin{aligned} &STL(f, Q, L_1, L_2, L_3, L_4, L_5, D_1, D_o, D_2, D_3) \\ &= 20 \log \left( \frac{|T11+T12+T21+T22|}{2} \right) + 10 \log \left( \frac{S_1}{S_5} \right) \\ &= STL(f, Q, L_1, L_3, L_5, L_2, L_o, D_1, D_o, D_2, D_3) \end{aligned} \quad (11a)$$

where

$$L_o = L_1 + L_2 + L_3 + L_4 + L_5 \quad (11b)$$

**Model Check**

Before performing both SA and GA optimal simulation on mufflers, the accuracy check of the mathematical model of a single-chamber muffler is performed with experimental data (Kim et al., 2002). As depicted in Figure 4, the accuracy comparison between the theoretical and experimental data for the models shows agreement. Therefore, the proposed mathematical model is acceptable. Consequently, the model linked with numerical methods is used for the shape optimization in the following section.

**Case Study**

The noise control of pure tone noise with 300 Hz is introduced as the numerical case. The available space for the muffler is  $0.5W * 0.5H * 3.0L$ . In Eq. (11),

7 design parameters are chosen for both the SA and GA optimizations. To avoid a larger pressure drop and a flow-generated noise, which normally occurs in mufflers (Schaffer and Mark, 1991), the minimal diameters (venting device) at D1, D2 and D3 are specified at no less than 0.0762 (m). In addition, each segment of the muffler is limited to not less than 0.1 (m) in order to facilitate better muffler quality.

A series of assumptions of the constrained condition in design are illustrated as

$$0.0762 \text{ (m)} \leq D_1 \leq 0.3 \text{ (m)}; 0.0762 \text{ (m)} \leq D_2 \leq 0.3 \text{ (m)}; 0.0762 \text{ (m)} \leq D_3 \leq 0.3 \text{ (m)}; 0.1 \text{ (m)} \leq L_1 \leq 0.2 \text{ (m)}; 0.1 \text{ (m)} \leq L_3 \leq 0.2 \text{ (m)}; 0.1 \text{ (m)} \leq L_5 \leq 0.2 \text{ (m)}; 0.1 \leq L_2 \leq 2 \text{ (m)}; L_o = 3.0 \text{ (m)}; D_o = 0.5 \text{ (m)}; Q = 0.8 \text{ (m}^3\text{/s)}; f = 300 \text{ (Hz)}$$

The space constraint for mufflers and the design volume flow rate are shown in Figure 5.

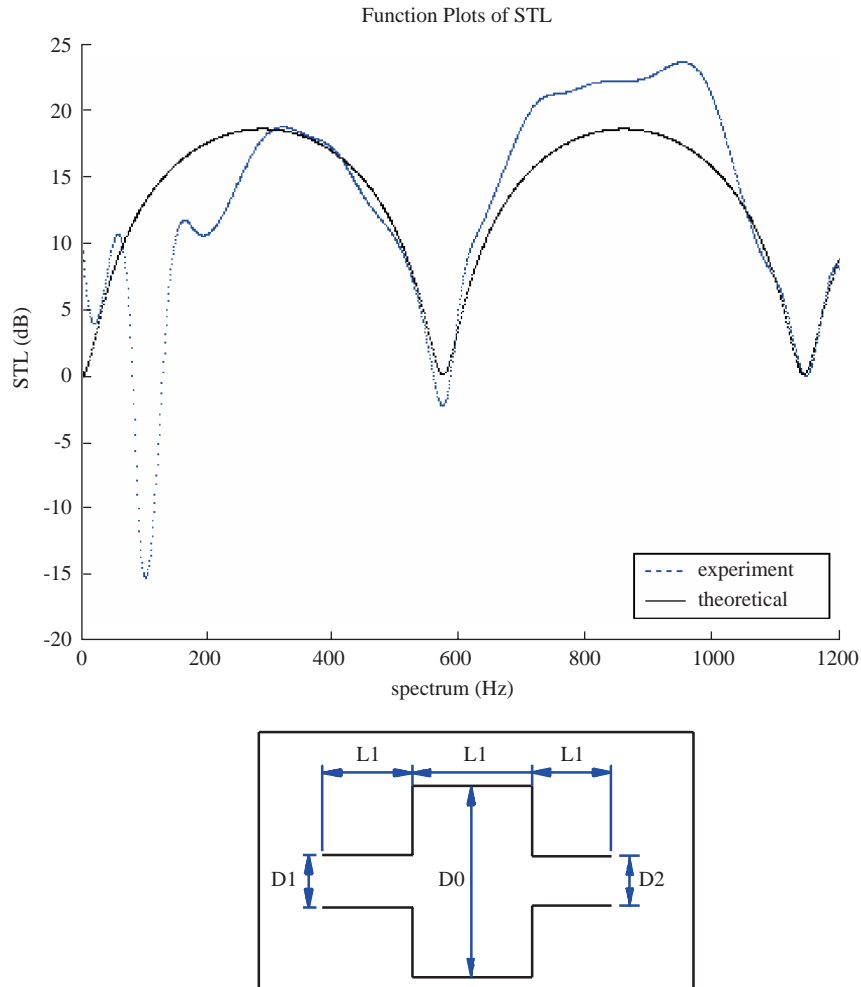


**Figure 4.** Performance of a single-chamber muffler without the mean flow [ $D_1 = D_2 = 0.0365\text{(m)}$ ,  $D_o = 0.15\text{(m)}$ ,  $L_1 = L_3 = 0.1\text{(m)}$ ,  $L_2 = 3\text{(m)}$ ].

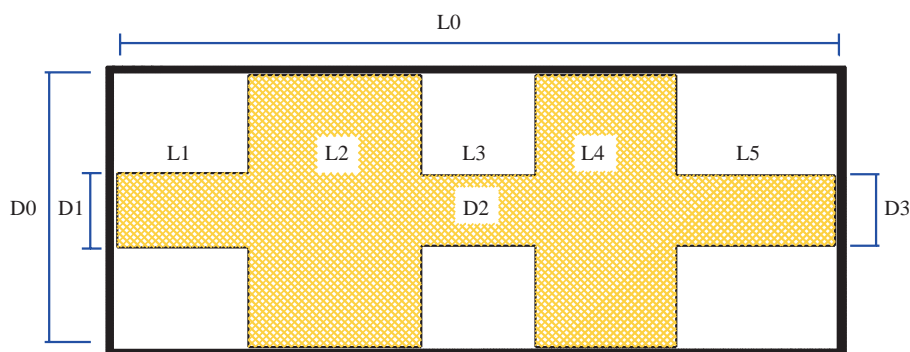


**Figure 5.** Space constraints for a double-chamber muffler [ $L_0 = 3.0(\text{m})$ ;  $D_0 = 0.5(\text{m})$ ].

## Optimization

### Simulated annealing

The SA algorithm, a local search process, simulates the softening process (annealing) of metal. In the physical system, annealing is the process of heating and keeping a metal at a stabilization temperature and cooling it slowly. Slow cooling allows the particles to keep their state close to the minimal energy state. In this state, the particles have a more uniform crystalline structure. However, a fast cooling rate (quenching) results in a higher energy condition with large internal energy stored inside the imperfect lattice. The basic concept behind SA was first introduced by Metropolis et al. (1953) and later developed by Kirkpatrick et al. (1983). The purpose of SA is to avoid stacking local optimal solutions during optimization.

The algorithm starts by generating a random initial solution. The scheme of the SA is a variation of the hill-climbing algorithm. All downhill movements for improvement are accepted for the decrement of the system energy. Simultaneously, SA also allows movement resulting in worse-quality solutions (uphill moves) than the current solution in order to escape from the local optimum. At higher temperatures, the uphill movement changes well. However, changes occurring when going uphill are decreased when the temperature drops.

To simulate the evolution of the SA algorithm, a new random solution is chosen from the neighborhood of the current solution. If the change in energy (or objective function) is negative, the new solution is accepted as the new current solution. Otherwise, the transition property ( $pb(T)$ ) of accepting the increment is computed by evaluating the Boltzmann's factor ( $pb(T) = \exp(\Delta F/CT)$ ) in which the  $\Delta F$ ,  $C$  and  $T$  are the difference of the objective func-

tion, Boltzmann constant and current temperature, respectively. To achieve an initial transition probability of 0.5, the initial temperature ( $T_o$ ) will be chosen at 0.2 (Nolle et al., 2002). If the probability is greater than a random number in the interval of  $[0,1]$ , the new solution is accepted. If not, it is rejected. The algorithm iterates the perturbation of the current solution and the measurement of the change in the objective function.

Each successful replacement of the new current solution leads to the decrement of the current temperature as

$$T_{new} = kk * T_{old}$$

where  $kk$  is the cooling rate chosen at 0.99 (Nolle et al., 2002). The process is repeated until the predetermined number ( $Iter_{max}$ ) of the outer loop is reached.

The flow diagram of SA optimization is described and shown in Figure 6. As indicated, the objective function in SA is represented by the negative value ( $-STL$ ) in order to maximize the STL on the muffler.

### Genetic algorithm

The concept of GAs, first formalized by Holland (1975), and extended to functional optimization by Jong (1975), later involved the use of optimization search strategies patterned after the Darwinian notion of natural selection and evolution. The GA accomplishes the task of optimization by starting with a random "population" of values for the parameters of an optimization problem. Thereafter, a new "generation" with improved values of the objective function is then produced. In order to achieve evolution in the new generation, the binary system is used. The binary system is a representation of real numbers and integers. In addition, by manipulating the strings, the operators of reproduction, crossover, mu-

tation and elitism are thus at work sequentially. A brief description of GA operators and their components is as follows:

**A. Populations and Chromosomes:** The initial population begins by randomization. The parameter set is encoded to form a string representing the chromosome. By evaluation of the objective function, each chromosome is assigned fitness.

**B. Parents:** By using the probabilistic computation weighted by the relative fitness, pairs of chromosome are selected as parents. Each individual in the population is assigned a space on the roulette wheel proportional to individual relative fitness. Individuals with the largest portion on the wheel have

the greatest probability of being selected as the parent generation for the next generation. A typical selection scheme of a weighted roulette wheel is depicted in Figure 7.

**C. Offspring:** One pair of offspring is generated from the selected parent by crossover. Crossover occurs with a probability of  $pc$ . Both the random selection of a crossover and the combination of the 2 parents' genetic data are then done. The scheme of single-point crossover is chosen from the GA optimization. Recombination and parent selection are the principle methods for the evolution of the GA. A typical scheme of single-point crossover is depicted in Figure 8.

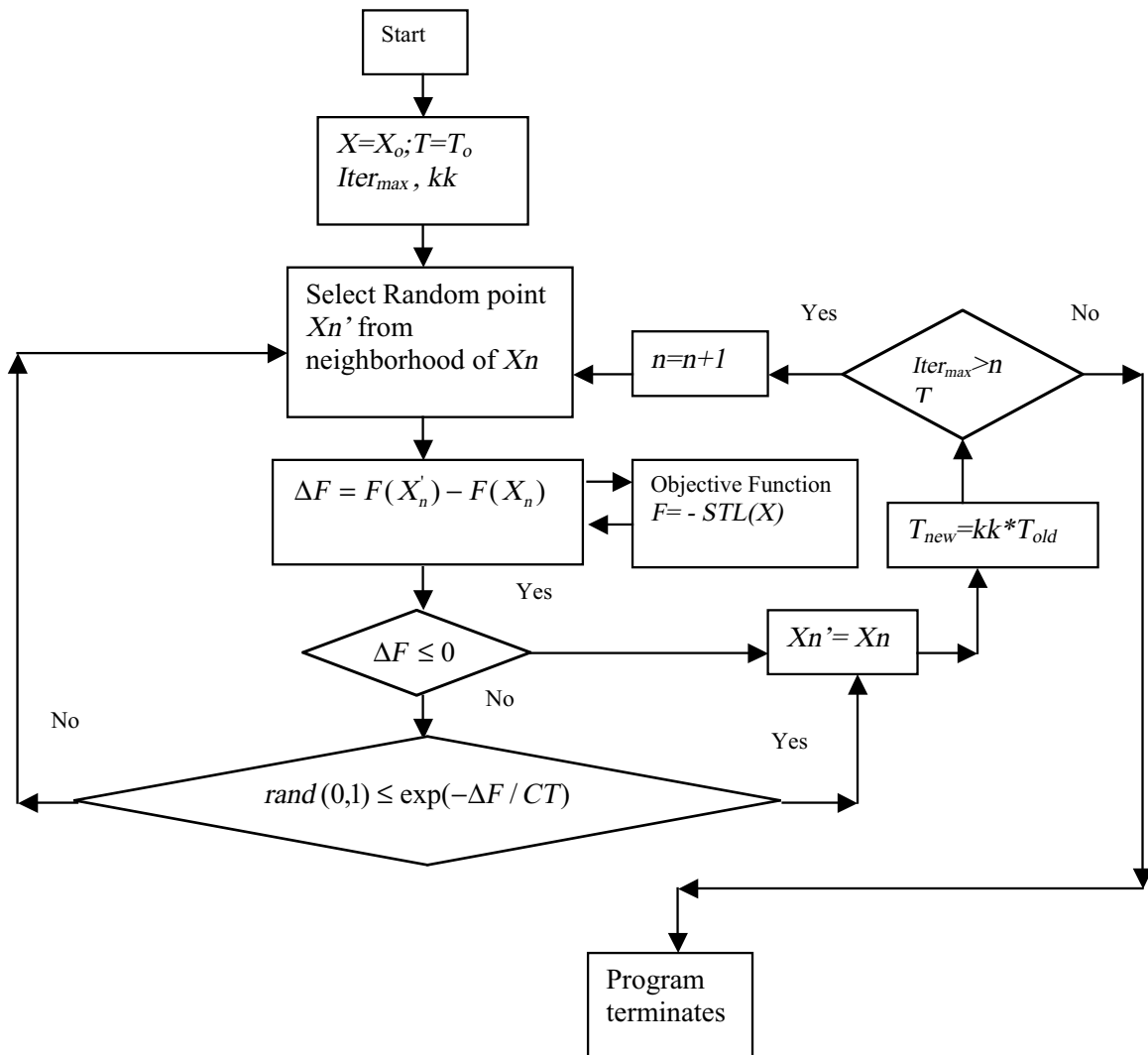
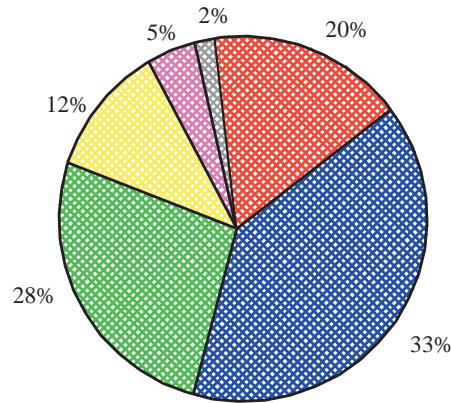


Figure 6. Flow diagram of SA optimization.

**D. Mutation:** The mutation operator is used to provide the needed diversity in the population and to search in different areas. Genetically, mutation occurs with a probability of  $pm$  wherein the new and unexpected point will be brought into the

GA optimizer's search domain. It is an essential operator that introduces diversity into the population and prevents the GA from becoming saturated with solutions in the local optimum. A typical scheme of mutation is depicted in Figure 9.



**Figure 7.** Weighted roulette wheel method of selection (ratio of individual relative fitness).

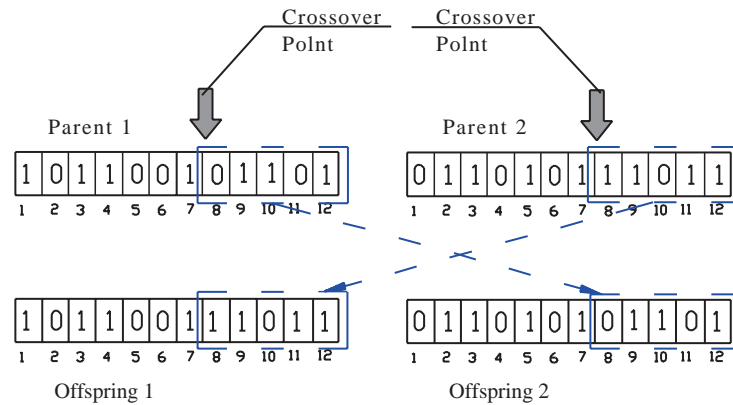


**Figure 8.** Scheme of single-point crossover.

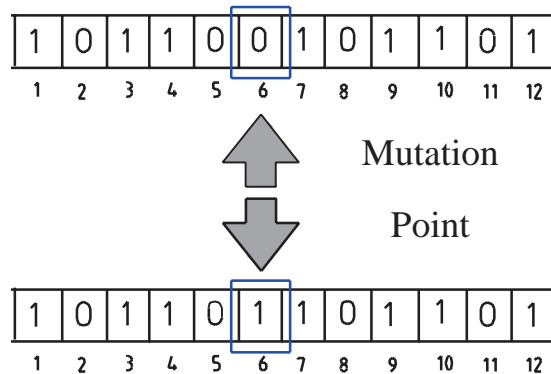


**Figure 9.** Scheme of mutation.

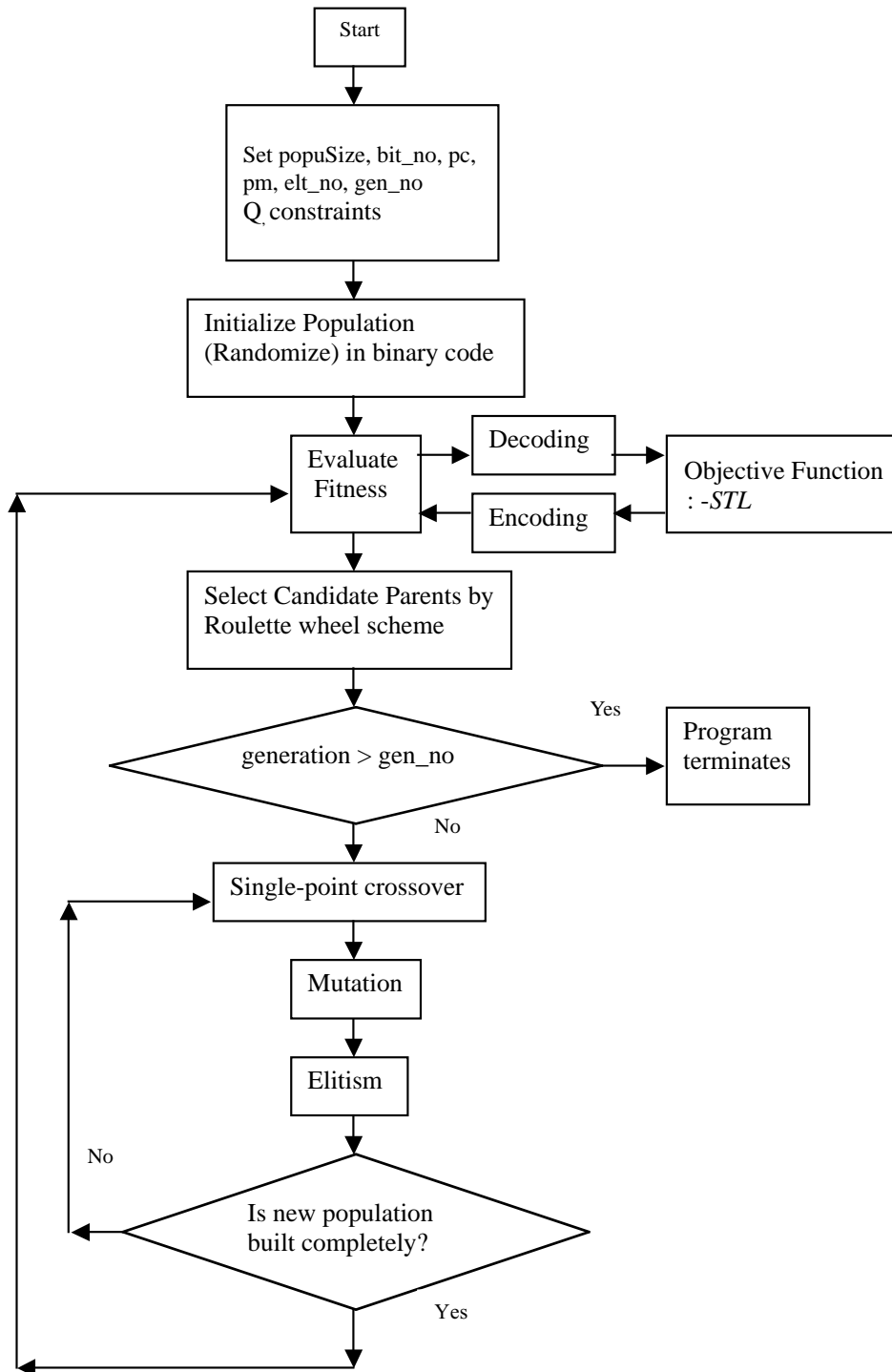


Figure 10. Block diagram of the GA optimization on mufflers.

**E. Elitism:** Elitism reintroduces the best candidate in each generation. It can prevent the best gene from disappearing and improves the accuracy of optimization during reproduction.

**F. New Generation:** Reproduction includes selection, crossover, mutation and elitism. The reduplication continues until a new generation is constructed and the original generation is substituted. Highly fit characteristics produce more copies of themselves in subsequent generations, resulting in a movement of the population towards an optimal direction. The process can be terminated when the number of predetermined maximum generations (*gen\_no*) has been reached. The block diagram of the GA optimization on mufflers is depicted in Figure 10.

## Results and Discussion

### Results

*SA:* The accuracy of the SA optimization depends on the cooling rate (*kk*) and the number of iteration (*Iter<sub>max</sub>*) (Cave et al., 2002). To identify the effect of the cooling rate and the number of iteration, an investigation of SA parameters, the cooling rate and the iteration is then carried out as follows:

**A. cooling rate** To achieve a better approach

in SA, 4 cooling rates (0.9, 0.95, 0.99 and 0.999) are tested at the maximal iteration number (*iter<sub>max</sub>*) of 50,000 and the initial temperature (*T<sub>o</sub>*) of 0.2. The results are summarized in Table 1. In addition, the annealing response curve with a cooling rate of 0.95 is demonstrated in Figure 11. As indicated in Table 1, the best result occurred at the higher cooling rate of 0.99. It reveals that the minimal state is achieved at the higher cooling rate.

Consequently, the acoustic performance of STL (with respect to frequency in the 4 design cases) is shown and plotted in Figure 12. Obviously, the best STL at the desired frequency of 300 Hz is found at the cooling rate of 0.99.

In the 4 cases, the calculations of SA optimization (run on an IBM PC - Pentium IV) are 7.81~8.42 min.

**B. iteration** To achieve a better approach in SA, 3 kinds of maximal iteration (5000, 50,000 and 80,000) are tested at the cooling rate of 0.99. The results are summarized in Table 2. In addition, the annealing response curve with an iteration number of 5000 is plotted in Figure 13. As indicated in Table 2, the best result occurred at the higher iteration number of 80,000. It is obvious that the minimal state (optimum) will be achieved at the higher iteration number.

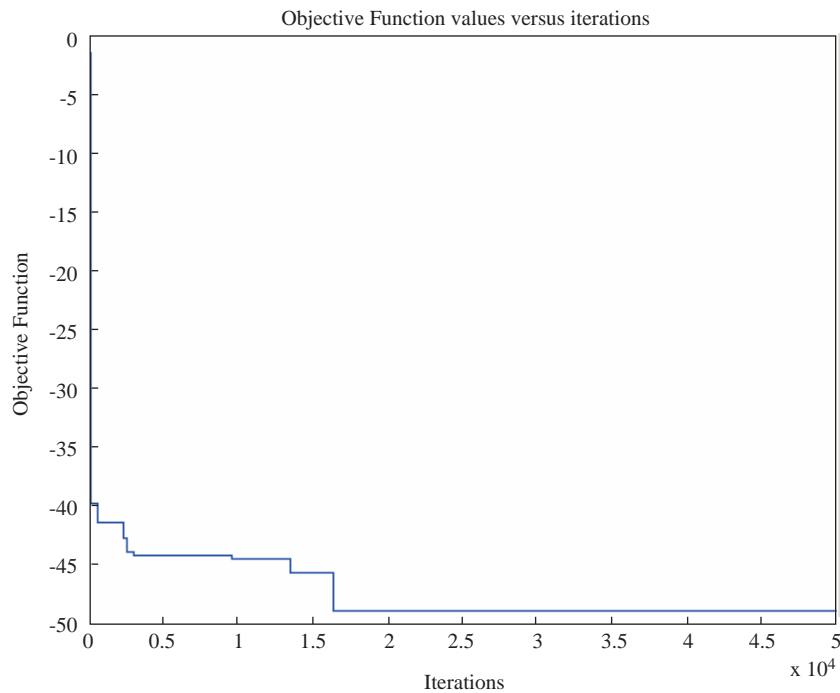


**Figure 11.** Annealing response at cooling rate (*kk*) of 0.95 [*T<sub>o</sub>* = 0.2; *iter<sub>max</sub>* = 50,000].

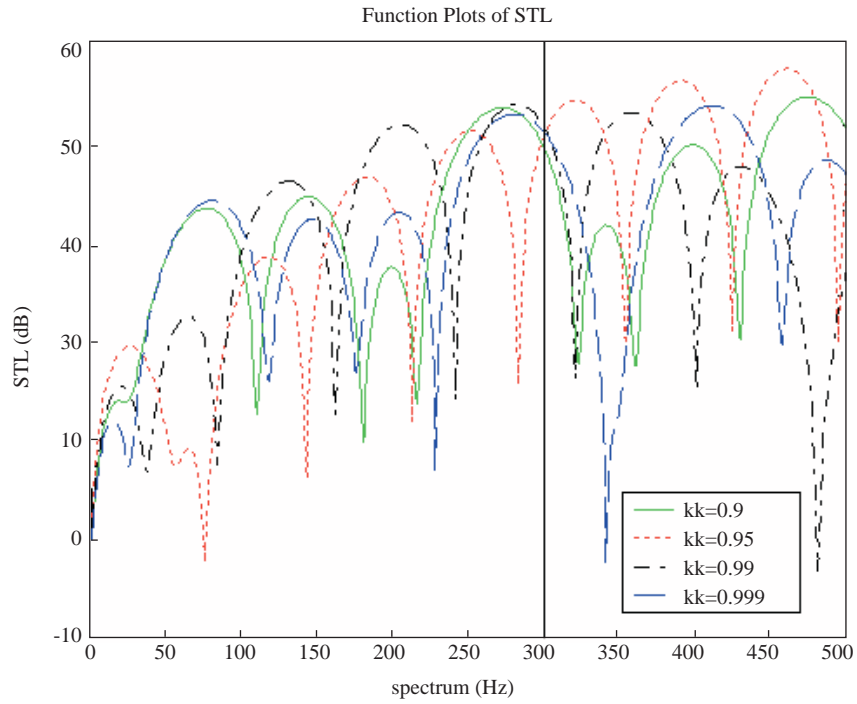


**Figure 12.** Performance curves of *STL* with respect to various cooling rates ( $kk$ ) by SA [ $T_o = 0.2$ ;  $iter_{\max} = 50,000$ ].

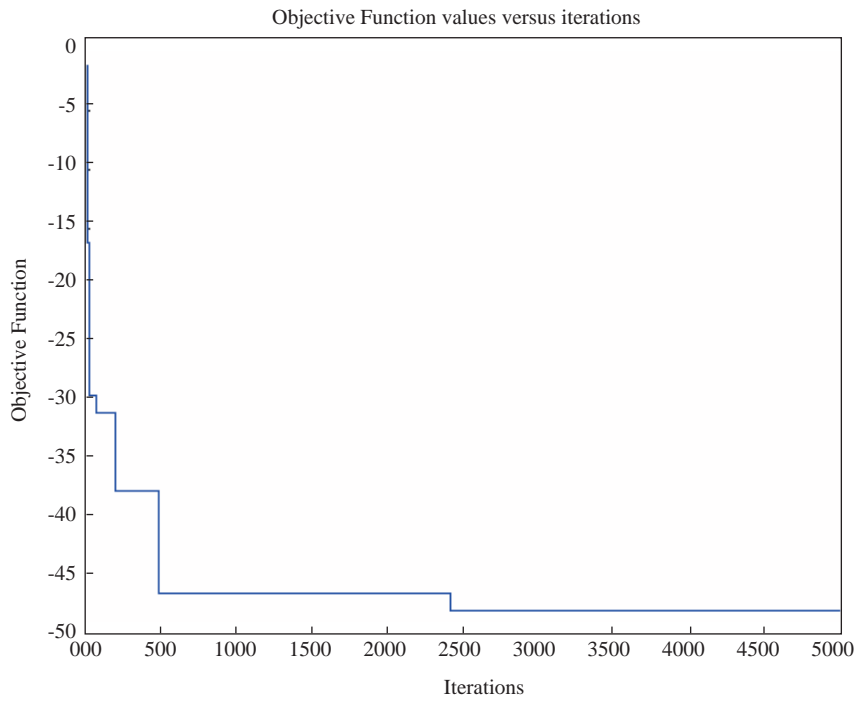


**Figure 13.** Annealing response at maximum iteration ( $iter_{\max}$ ) of 5000 [ $T_o = 0.2$ ;  $kk = 0.99$ ].

Consequently, the acoustic performance of STL (with respect to frequency in 3 design cases) is shown and plotted in Figure 14. Obviously, the best value

of STL at 300 Hz is found at the iteration number of 80,000, whereas the longer time requirement of 22.16 min is compared to other cases.

**Table 1.** Results of *STL* at pure tone noise of 300 Hz in 4 cases of various cooling rates (*kk*) by SA.

Common parameters		Control parameters	Results								Elapsed time
$T_o$	$iter_{max}$	<i>kk</i>	$D_1$ (m)	$D_2$ (m)	$D_3$ (m)	$L_1$ (m)	$L_3$ (m)	$L_5$ (m)	$L_2$ (m)	<i>STL</i>	t(Min.)
0.2	50,000	0.9	0.0917	0.0835	0.0933	0.1578	0.1787	0.1156	1.5984	47.5	7.95
0.2	50,000	0.95	0.0773	0.0763	0.0772	0.1299	0.1871	0.1532	0.1035	48.8	8.08
0.2	50,000	0.99	0.1041	0.0814	0.0766	0.1494	0.1619	0.1913	0.3543	49.9	8.0
0.2	50,000	0.999	0.1004	0.0828	0.0938	0.1920	0.1879	0.1315	0.9884	49.3	8.42

**Table 2.** Results of *STL* at pure tone noise of 300 Hz in 4 cases of various maximal iteration ( $iter_{max}$ ) by SA.

Common parameters		Control parameters	Results								Elapsed time
$T_o$	<i>kk</i>	$iter_{max}$	$D_1$ (m)	$D_2$ (m)	$D_3$ (m)	$L_1$ (m)	$L_3$ (m)	$L_5$ (m)	$L_2$ (m)	<i>STL</i>	t(Min.)
0.2	0.99	5000	0.1228	0.0823	0.1117	0.1789	0.1979	0.1570	0.4055	47.1	0.21
0.2	0.99	50,000	0.1041	0.0814	0.0766	0.1494	0.1619	0.1913	0.3543	49.9	8.0
0.2	0.99	80,000	0.0802	0.0818	0.0762	0.1585	0.1915	0.1174	1.5636	52.3	22.16

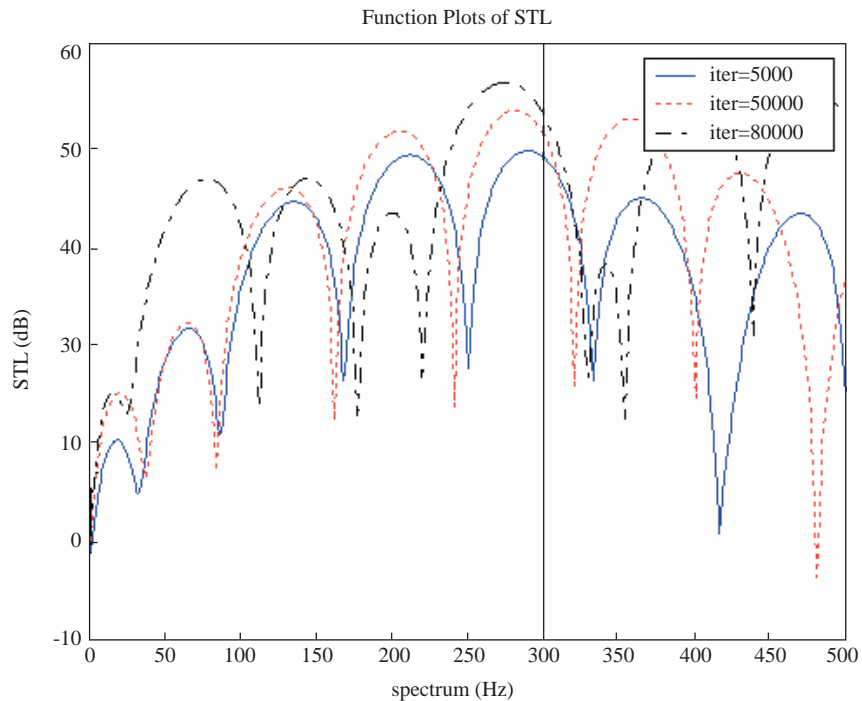


**Figure 14.** Performance curves of *STL* with respect to various maximal iterations ( $iter_{max}$ ) by SA [ $T_o = 0.2$ ;  $kk = 0.99$ ].

### GA operator

The GA parameters of crossover mutation and elitism with respect to 0.8, 0.05 and 1 are chosen and applied in the following optimization. To identify the effect of the iteration number in the generation, the investigation in the predetermined maximal generation (*gen\_no*) is then carried out as follows.

To achieve a better approach in GA, 2 kinds of maximal generation number (*gen\_no*)(5000 and 50,000) are tested. The results are summarized in Table 3. In addition, the response curve with maximal generation of 5000 is depicted in Figure 15. As indicated in Table 3, the best result occurred at the higher generation number (*gen\_no*) of 50,000.

### Discussion

As described above both the cooling rate (*kk*) and the maximal iteration (*iter\_max*) play essential roles in SA optimization. The good value of the cooling rate (*kk*) is found at 0.99. In addition, the accuracy of the SA highly depends on the number of iteration (*iter\_max*). A higher number of iteration (*iter\_max*)

improves the acoustic performance of STL. The computation time also increases simultaneously.

The investigation of a generation in GA is carried out and shown in Table 3. Even though the numbers of the generation are increased from 500 to 5000, the variation of optimal STL is about 0.005 (small enough to be ignored). This means that the chosen number of generation at 500 is adequate for the purpose of accuracy in the GA.

To check the accuracy between SA and the GA, both the maximal iteration (*iter\_max*) in SA and the maximal generation (*gen\_no*) in the GA are chosen at the value of 5000.

The acoustic performances of STL (optimized by SA and the GA at the same iteration of 5000) are plotted in Figure 16. The GA has the better STL at the desired frequency of 300 Hz than SA.

Furthermore, the best results in SA (with  $T_o=0.2$ ,  $kk=0.99$  and  $iter_{max}=80,000$ ) and the GA (with  $pc=0.8$ ,  $pm=0.05$ ,  $elit_{no}=1$  and  $gen_{no}=5000$ ) translate into related physical shapes (as shown in Figures 17 and 18 respectively). In addition, the running times of SA and the GA were 22.16 and 12.1 min, respectively.

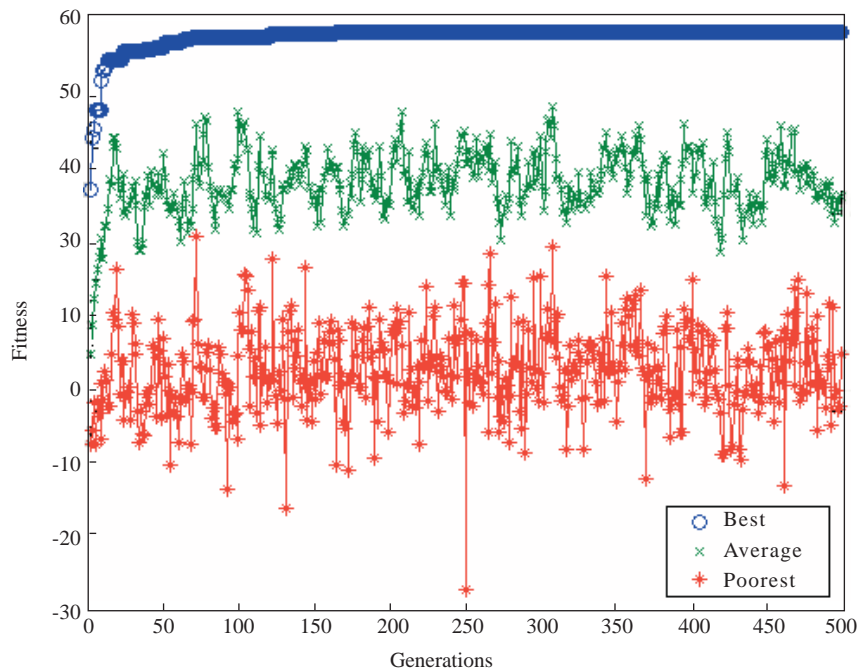


**Figure 15.** Annealing response at maximum generation (*gen\_no*) of 5000 by GA [ $pc=0.8$ ;  $pm=0.05$ ;  $elit_{no}=1$ ].

**Table 3.** Results of STL at pure tone noise of 300 Hz in 2 cases of various maximal generation (*gen\_no*) by GA.

Common parameters			Control parameters			Results								Elapsed time
<i>popuSize</i>	<i>gen_no</i>	<i>bit_no</i>	<i>pc</i>	<i>pm</i>	<i>elt_no</i>	$D_1$ (m)	$D_2$ (m)	$D_3$ (m)	$L_1$ (m)	$L_3$ (m)	$L_5$ (m)	$L_2$ (m)	<i>STL</i>	t(Min.)
60	500	40	0.8	0.05	1	0.0762	0.0762	0.0762	0.1992	0.1998	0.1995	0.3437	57.5	1.18
60	5000	40	0.8	0.05	1	0.0762	0.0762	0.0762	0.1999	0.1999	0.1999	0.3374	57.6	12.1

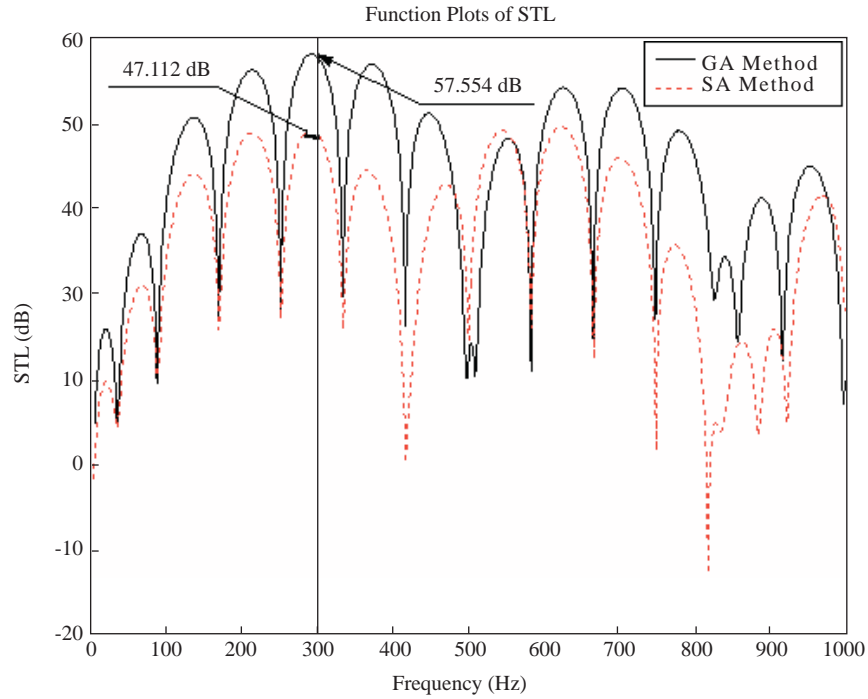


**Figure 16.** Comparison of performance curves of *STL* between SA and GA on the basis of same iterations of 5000 [SA:  $T_o = 0.2$ ,  $kk = 0.99$ ; GA:  $pc = 0.8$ ,  $pm = 0.05$ ,  $elt\_no = 1$ ].

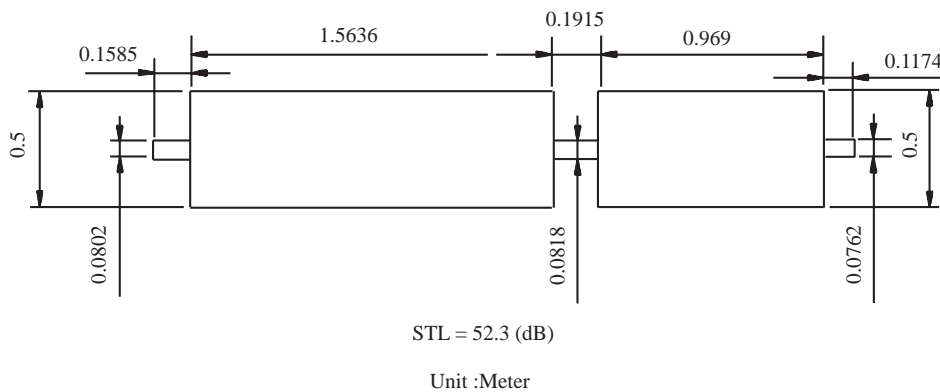
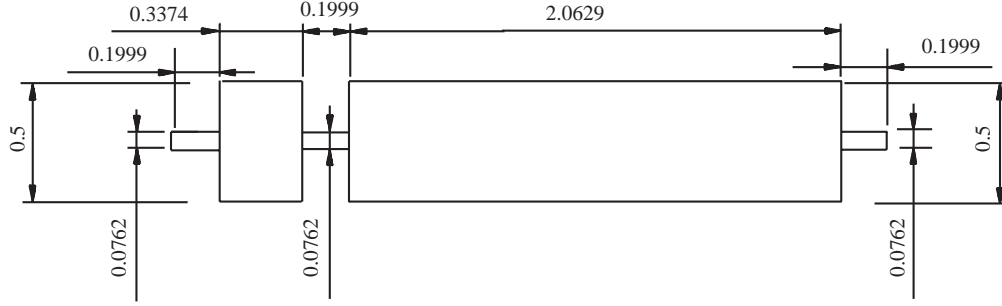


**Figure 17.** Optimal shape of muffler with respect to the best design set by SA [SA parameters:  $T_o = 0.2$ ,  $iter_{max} = 80,000$ ,  $kk = 0.99$ ].



STL = 57.6 (dB)

Unit: Meter

**Figure 18.** Optimal shape of muffler with respect to the best design set by GA [GA parameters:  $pc = 0.8$ ,  $pm = 0.05$ ,  $elt\_no = 1$ ,  $gen\_no = 5000$ ].

### Conclusion

It has been shown that both SA and a GA can be used in the shape optimization of double-chamber mufflers by adjusting the shape of the muffler under space constraints. Both the cooling rate ( $kk$ ) and the iteration number ( $iter_{max}$ ) play essential roles in SA optimization. By increasing the values of the cooling rate and the iteration in SA, the acoustic performance of STL can be significantly improved. In order to achieve more accurate results, more time should be spent in simulating larger iteration. In addition, using the operators of crossover, mutation and elitism, GA optimization is carried out well. Under the same iteration (or generation), the simulated results of STL with respect to SA and the GA are compared. The result reveals that the GA has a better acoustic performance than SA.

Nevertheless, both the SA and the GA are much easier to use compared to gradient-based optimizers, wherein good starting points are required. The case study reveals that either SA or the GA is applicable in the shape optimization of double-chamber mufflers under space constraints.

### Nomenclature

$bit\_no$	bit length
$C_o$	sound speed ( $m\ s^{-1}$ )
$D$	diameter (m)
$elt\_no$	selection of elite (1 for yes and 0 for no)
$f$	cyclic frequency (Hz)
$gen\_no$	maximum number of generation
$iter_{max}$	maximum iteration in SA

$j$	imaginary unit ( $\sqrt{-1}$ )
$J_m$	Bessel function of order $m$
$k$	wave number ( $w/c_o$ )
$kk$	cooling rate in SA
$k_{r,m,n}^{\pm}$	wave number in r-direction
$k_{z,m,n}^{\pm}$	wave number in z-direction
$L$	length of the $i$ th segment of straight duct (m)
$M_i$	mean flow Mach number at the $i$ th segment of straight duct
$pc$	crossover ratio
$p_i$	pressure; acoustic pressure at $i$ (Pa)
$pm$	mutation ratio
$popuSize$	number of population
$Q$	volume flow rate of venting gas ( $m^3\ s^{-1}$ )
$S_i$	section area at $i$ ( $m^2$ )
$SPL_o$	sound pressure level at the silencer inlet (dB(A))
$SPL_T$	sound pressure level at the silencer outlet (dB(A))
$STL$	sound transmission loss (dB)
$T_o$	initial temperature
$u_i$	acoustic particle velocity at $i$ ( $m\ s^{-1}$ )
$v_i$	acoustic mass velocity at $i$ ( $kg\ s^{-1}$ )
$\rho_o$	air density ( $kg\ m^{-3}$ )
$\nabla$	gradient vector
$\nabla^2$	Laplacian

### Acknowledgments

The authors acknowledge the financial support of the National Science Council (NSC91-2622-E-036-002-CC32), ROC.

References

- Cave, A., Nahavandi, S. and Kouzani, A., "Simulation Optimization for Process Scheduling through Simulated Annealing", Proceedings of the Winter Simulation Conference, 1909-1913, 2002.
- Cheremisinoff, P.N. and Cheremisinoff, P.P., Industrial Noise Control Handbook, Ann Arbor Science, Michigan, 1977.
- Holland, J.H., Adaptation in Natural and Artificial System, Ann Arbor, MI, The University of Michigan Press, 1975.
- Jong, D., Analysis of the Behavior of a Class of Genetic Adaptive Systems, PhD Dissertation, The University of Michigan Press, 1975.
- Kim, Y.H., Choi, J.W. and Lim, B.D., "Acoustic Characteristics of an Expansion Chamber with Constant Mass Flow and Steady Temperature Gradient (Theory and Numerical Simulation)", Journal of Vibration and Acoustics, 112, 460-467, 1990.
- Kirkpatrick, S., Gelatt, C.D., Jr. and Vecchi, M.P., "Optimization by Simulated Annealing", Science, 220, 4598, 671-680, 1983.
- Magrab, E.B., Environmental Noise Control, John Wiley & Sons, New York, 1975.
- Metropolis, A., Rosenbluth, W., Rosenbluth, M.N., Teller, H. and Teller, E., "Equation of Static Calculations by Fast Computing Machines", The Journal of Chemical Physics, 21, 6, 1087-1092, 1953.
- Munjal, M.L., Acoustics of Ducts and Mufflers with Application to Exhaust and Ventilation System Design, John Wiley & Sons, New York, 1987.
- Nolle, L., Armstrong, D.A., Hopgood, A.A. and Ware, J.A., "Simulated Annealing and Genetic Algorithms Applied to Finishing Mill Optimization for Hot Rolling of Wide Steel Strip", International of Knowledge-Based Intelligent Engineering System, 6, 2, 104-111, 2002.
- Schafer, M.E., A Practical Guide to Noise and Vibration Control for HVAC Systems, ASHRAE, New York, 1991.
- Yeh, L.J., Chiu, M.C. and Lai, G.J., "Computer Aided Design on Single Expansion Muffler under Space Constraints", Proc. Nineteenth C.S.M.E. National Conf., Taiwan, ROC, 625-633, 2002.
- Yeh, L.J., Chang, Y.C., Chiu, M.C., Lai, G.J. and Her, M.G., "Shape Optimization of Constrained Double-chamber Muffler with Extended Tubes by Mathematical Gradient Methods", Proceedings of the 3<sup>rd</sup> Conference on S.M.E., Taiwan, ROC, 519-526, 2003.

APPENDIX A

Transfer Matrix of Straight Duct

For a 3-dimensional wave with moving medium, 3 kinds of governing equations are

I. Mass continuity equation:

$$\rho_o \nabla \cdot \vec{u} + \frac{D\rho}{Dt} = 0 \tag{A1}$$

II. Momentum equation:

$$\rho_o \frac{D\vec{u}}{Dt} + \nabla p = 0 \tag{A2}$$

III. Energy equation (isentropic):

$$\left( \frac{\partial p}{\partial \rho} \right)_s = \frac{\gamma(p_o + p)}{\rho_o + \rho} \approx \frac{\gamma p_o}{\rho_o} = c_o^2 \text{ or } \frac{p}{\rho} = c_o^2 \tag{A3}$$

By partial derivation and substitution in Eqs. (A1), (A2) and (A3), the wave governing equation yields

$$\left(\frac{D^2}{Dt^2} - c_o^2 \nabla^2\right) p = 0 \quad (\text{A4})$$

By using the separation of variables method in Eqs. (A4), it yields

$$p(r, \theta, z, t) = \sum_{m=0}^{\infty} \sum_{n=0}^{\infty} J_m(k_{r,m,n} r) \left( C_{1,m,n} e^{-jk_{z,m,n}^+ z} + C_{2,m,n} e^{+jk_{z,m,n}^- z} \right) e^{j\omega t} \quad (\text{A5})$$

$$\begin{aligned} u_z(r, \theta, z, t) \\ = \frac{1}{\rho_o c_o} \sum_{m=0}^{\infty} \sum_{n=0}^{\infty} J_m(k_{r,m,n} r) e^{jm\theta} e^{j\omega t} \left( \begin{aligned} & \frac{k_{z,m,n}^+}{k_o - M k_{z,m,n}^+} C_{1,m,n} e^{-jk_{z,m,n}^+ z} \\ & + \frac{k_{z,m,n}^-}{k_o + M k_{z,m,n}^-} C_{2,m,n} e^{+jk_{z,m,n}^- z} \end{aligned} \right) \end{aligned} \quad (\text{A6})$$

$$k_{z,m,n}^{\pm} = \frac{\mp M_1 k_o + [k_o^2 - (1 - M_1^2) k_{r,m,n}^2]^{1/2}}{1 - M_1^2} \quad (\text{A7})$$

For the fundamental mode of ( $m = 0, n = 0$ ), only a plane wave would propagate if the frequencies of  $f$  are smaller than both of the diametral cut-off frequency  $-f_{c1}$  and the axisymmetric radial cut-off frequency  $-f_{c2}$  . where

$$f_{c1} = \frac{1.84 c_o}{\pi D} (1 - M_1^2)^{1/2}; \quad f_{c2} = \frac{3.83 c_o}{\pi D} (1 - M_1^2)^{1/2} \quad (\text{A8})$$

For one-dimensional wave propagating in a symmetric straight duct, the acoustic pressure and particle velocity are reduced as

$$p(z, t) = \left( C_1 e^{-jk_o z / (1+M_1)} + C_2 e^{+jk_o z / (1-M_1)} \right) e^{j\omega t} \quad (\text{A9})$$

$$u(z, t) = \left( \frac{C_1}{\rho_o c_o} e^{-jk_o z / (1+M_1)} - \frac{C_2}{\rho_o c_o} e^{+jk_o z / (1-M_1)} \right) e^{j\omega t} \quad (\text{A10})$$

By taking boundary conditions of point 1 ( $z = 0$ ) and point 2 ( $z = L$ ) into Eqs. (A10) and (A11), it yields

$$\begin{pmatrix} p_1 \\ \rho_o c_o u_1 \end{pmatrix} = \begin{bmatrix} 1 & 1 \\ 1 & -1 \end{bmatrix} \begin{pmatrix} C_1 \\ C_2 \end{pmatrix} \quad (\text{A11})$$

$$\begin{pmatrix} p_2 \\ \rho_o c_o u_2 \end{pmatrix} = \begin{bmatrix} e^{-jk^+ L_1} & e^{+jk^- L_1} \\ e^{-jk^+ L_1} & -e^{+jk^- L_1} \end{bmatrix} \begin{pmatrix} C_1 \\ C_2 \end{pmatrix} \quad (\text{A12})$$

where  $k^+ = \frac{k_o}{1+M_1}; k^- = \frac{k_o}{1-M_1}$

Combination of Eqs. (A11) and (A12) gives

$$\begin{aligned} \begin{pmatrix} p_1 \\ \rho_o c_o u_1 \end{pmatrix} &= e^{-j \frac{M_1 k L}{1-M_1^2}} \begin{bmatrix} \cos\left(\frac{k L_1}{1-M_1^2}\right) & j \sin\left(\frac{k L_1}{1-M_1^2}\right) \\ j \sin\left(\frac{k L_1}{1-M_1^2}\right) & \cos\left(\frac{k L_1}{1-M_1^2}\right) \end{bmatrix} \begin{pmatrix} p_2 \\ \rho_o c_o u_2 \end{pmatrix} \\ &= e^{-j \frac{M_1 k L}{1-M_1^2}} \begin{bmatrix} b_{11} & b_{12} \\ b_{21} & b_{22} \end{bmatrix} \begin{pmatrix} p_2 \\ \rho_o c_o u_2 \end{pmatrix} \end{aligned} \quad (\text{A13a})$$

where

$$b_{11} = \cos\left(\frac{k L_1}{1-M_1^2}\right); b_{12} = j \sin\left(\frac{k L_1}{1-M_1^2}\right); b_{21} = j \sin\left(\frac{k L_1}{1-M_1^2}\right); b_{22} = \cos\left(\frac{k L_1}{1-M_1^2}\right) \quad (\text{A13b})$$

As the derivation in Eq. (A13), the 4-pole matrix between point 3 and point 4 with mean flow is expressed in equation (A14).

$$\begin{pmatrix} p_3 \\ \rho_o c_o u_3 \end{pmatrix} = e^{-j M_2 k L_2 / (1-M_2^2)} \begin{bmatrix} c_{11} & c_{12} \\ c_{21} & c_{22} \end{bmatrix} \begin{pmatrix} p_4 \\ \rho_o c_o u_4 \end{pmatrix} \quad (\text{A14a})$$

where

$$c_{11} = \cos\left(\frac{k L_2}{1-M_2^2}\right); c_{12} = j \sin\left(\frac{k L_2}{1-M_2^2}\right); c_{21} = j \sin\left(\frac{k L_2}{1-M_2^2}\right); c_{22} = \cos\left(\frac{k L_2}{1-M_2^2}\right) \quad (\text{A14b})$$

Thus, the 4-pole matrix between point 5 and point 6 with mean flow is expressed in equation (A15).

$$\begin{pmatrix} p_5 \\ \rho_o c_o u_5 \end{pmatrix} = e^{-j M_3 k L_3 / (1-M_3^2)} \begin{bmatrix} d_{11} & d_{12} \\ d_{21} & d_{22} \end{bmatrix} \begin{pmatrix} p_6 \\ \rho_o c_o u_6 \end{pmatrix} \quad (\text{A15a})$$

where

$$d_{11} = \cos\left(\frac{k L_3}{1-M_3^2}\right); d_{12} = j \sin\left(\frac{k L_3}{1-M_3^2}\right); d_{21} = j \sin\left(\frac{k L_3}{1-M_3^2}\right); d_{22} = \cos\left(\frac{k L_3}{1-M_3^2}\right) \quad (\text{A15b})$$

Obviously, the 4-pole matrix between point 7 and point 8 with mean flow is expressed in equation (A16).

$$\begin{pmatrix} p_7 \\ \rho_o c_o u_7 \end{pmatrix} = e^{-j M_4 k L_4 / (1-M_4^2)} \begin{bmatrix} e_{11} & e_{12} \\ e_{21} & e_{22} \end{bmatrix} \begin{pmatrix} p_8 \\ \rho_o c_o u_8 \end{pmatrix} \quad (\text{A16a})$$

where

$$e_{11} = \cos\left(\frac{k L_4}{1-M_4^2}\right); e_{12} = j \sin\left(\frac{k L_4}{1-M_4^2}\right); e_{21} = j \sin\left(\frac{k L_4}{1-M_4^2}\right); e_{22} = \cos\left(\frac{k L_4}{1-M_4^2}\right) \quad (\text{A16b})$$

The 4-pole matrix between point 9 and point 10 with mean flow is expressed in equation (A17).

$$\begin{pmatrix} p_9 \\ \rho_o c_o u_9 \end{pmatrix} = e^{-j M_5 k L_5 / (1-M_5^2)} \begin{bmatrix} f_{11} & f_{12} \\ f_{21} & f_{22} \end{bmatrix} \begin{pmatrix} p_{10} \\ \rho_o c_o u_{10} \end{pmatrix} \quad (\text{A17a})$$

where

$$f_{11} = \cos\left(\frac{kL_5}{1 - M_5^2}\right); f_{12} = j \sin\left(\frac{kL_5}{1 - M_5^2}\right); f_{21} = j \sin\left(\frac{kL_5}{1 - M_5^2}\right); f_{22} = \cos\left(\frac{kL_5}{1 - M_5^2}\right) \quad (\text{A17b})$$

## APPENDIX B

### Transfer Matrix of a Simple Expansion/Contraction Duct

For a one-dimensional plane wave, acoustic pressure  $p$  and acoustic mass velocity  $v (= \rho_o S u)$  remain the same across either of the 2 discontinuities of point 2 or point 3. Thus,

$$p_2 = p_3; \quad v_2 = v_3; \quad (\text{B1})$$

The relationships between point 2 and point 3 in matrix form is

$$\begin{pmatrix} p_2 \\ v_2 \end{pmatrix} = \begin{bmatrix} 1 & 0 \\ 0 & 1 \end{bmatrix} \begin{pmatrix} p_3 \\ v_3 \end{pmatrix} \quad (\text{B2})$$

By the replacement of  $v$  into  $u$ , the transfer matrix for equation (B2) is

$$\begin{pmatrix} p_2 \\ \rho_o c_o u_2 \end{pmatrix} = \begin{bmatrix} 1 & 0 \\ 0 & \frac{S_2}{S_1} \end{bmatrix} \begin{pmatrix} p_3 \\ \rho_o c_o u_3 \end{pmatrix} \quad (\text{B3})$$

As derived in Eq.(B3), the relationships between point 4 and point 5 in matrix form is

$$\begin{pmatrix} p_4 \\ \rho_o c_o u_4 \end{pmatrix} = \begin{bmatrix} 1 & 0 \\ 0 & \frac{S_3}{S_2} \end{bmatrix} \begin{pmatrix} p_5 \\ \rho_o c_o u_5 \end{pmatrix} \quad (\text{B4})$$

and the relationships between point 6 and point 7 in matrix form is

$$\begin{pmatrix} p_6 \\ \rho_o c_o u_6 \end{pmatrix} = \begin{bmatrix} 1 & 0 \\ 0 & \frac{S_4}{S_3} \end{bmatrix} \begin{pmatrix} p_7 \\ \rho_o c_o u_7 \end{pmatrix} \quad (\text{B5})$$

Finally, the relationships between point 8 and point 9 in matrix form is

$$\begin{pmatrix} p_8 \\ \rho_o c_o u_8 \end{pmatrix} = \begin{bmatrix} 1 & 0 \\ 0 & \frac{S_5}{S_4} \end{bmatrix} \begin{pmatrix} p_9 \\ \rho_o c_o u_9 \end{pmatrix} \quad (\text{B6})$$